Satellite Products and Services Review Board

Algorithm Theoretical Basis Document

Enterprise Fractional Snow Cover Map Product

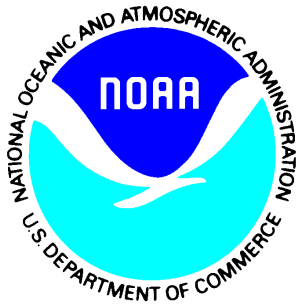

Version 1.0

June 2020

TITLE: ALGORITHM THEORETICAL BASIS DOCUMENT: ENTERPRISE FRACTIONAL SNOW COVER PRODUCT

AUTHOR:

Peter Romanov (NOAA-CREST, City University of New York)

DOCUMENT HISTORY
DOCUMENT REVISION LOG

The Document Revision Log identifies the series of revisions to this document since the baseline release. Please refer to the above page for version number information.

DOCUMENT TITLE: Algorithm Theoretical Basis Document: VIIRS Binary Snow Cover Product			
DOCUMENT CHANGE HISTORY			
Revision No.	**Date**	**Revision Originator Project Group**	**CCR Approval # and Date**
1.0	06/17/2020	No version 0	N/A

LIST OF CHANGES

Significant alterations made to this document are annotated in the List of Changes table.

DOCUMENT TITLE: Algorithm Theoretical Basis Document: VIIRS Binary Snow Cover Product					
LIST OF CHANGE-AFFECTED PAGES/SECTIONS/APPENDICES					
Version Number	**Date**	**Changed By**	**Page**	**Section**	**Description of Change(s)**

TABLE OF CONTENTS

LIST OF TABLES AND FIGURES

Page

1. INTRODUCTION

Snow and ice cover are among the key Earth's surface characteristics influencing radiation budget, energy exchange between the land surface or ocean and the atmosphere, and water balance. Information on the spatial extent and distribution of snow and ice cover presents an important input to numerical weather prediction (NWP), hydrological and climate models. Satellites present one of important sources of information on snow. High spatial resolution, wide area coverage and short revisit time allow for efficient, spatially detailed monitoring of both seasonal and perennial snow cover over the globe.

Although the albedo of pure snow may exceed 0.9, the albedo of natural snow-covered surfaces rarely reaches such high values. First, the snow pack, particularly during the snowmelt may develop a patchy pattern which brings down the reflectance of the mixed surface. Second, snow cover is often littered by vegetation debris or masked by the canopy. Because of these factors only a portion of the snow covered area may be directly exposed to the atmosphere and thus contributes to the reflective properties of the land surface. To properly account for fractional feature of the snow cover and for the masking effect of the vegetation when estimating the reflective properties of the land surface and in particular, its albedo, information on the snow cover fraction is needed.

A large number of existing and future satellite sensors onboard operational polar orbiting and geostationary weather satellites provide daily observations of the Earth's surface in the visible, near-infrared, shortwave infrared, middle infrared and in the far infrared spectral bands. Observations with this set of spectral bands is sufficient for establishing an automated algorithm for snow cover identification and hence for providing routine mapping and monitoring of the global snow cover. Global daily observations are available at high, up to 375m spatial resolution from polar orbiting satellites and at up to 1 km resolution from geostationary satellites. This allows for detailed characterization of the snow cover distribution on the ground surface with remote sensing data. Besides a simple binary snow cover classification where every pixel is flagged as either snow covered or snow free, these observations provide potentials for estimating the portion of the pixel affected by the snow cover and thus to derive a subpixel snow cover fraction.

This document presents the description of the Enterprise Fractional Snow Cover product and of the corresponding Enterprise Binary Snow retrieval algorithm. This is a universal algorithm that is supposed to be used with observations from all operational polar orbiting and geostationary satellites at NESDIS. At this time the algorithm is applied to observations from the Visible Infrared Imaging Radiometer Suite (VIIRS) onboard SNPP and JPSS satellites. In the future it will be also used with the data from MetImage instrument onboard

METOP Second Generation (SG) satellites. The Enterprise Fractional Snow Cover algorithm is also planned for implementation with the Advanced Baseline Imager (ABI) of GOES-R series geostationary satellites, however in the latter case a number of modifications will be needed accounting for a completely different observation geometry.

1.1. Product Overview

1.1.1. Product Description

The Enterprise Fractional Snow Cover Map Product (or Snow Fraction) characterizes the portion of the ground surface covered with snow as it is seen from the satellite. In other words, the derived parameter represents the “viewable snow fraction” which accounts both for the patchy structure of the snow pack and for the masking of the snow cover by the tree canopy. The snow cover fraction is estimated with two different algorithms. The first algorithm as adopted from MODIS and assumes a linear relationship between the snow fraction and the Normalized Difference Snow Index (NDSI). The second algorithm assumes that the snow fraction is linearly related to the visible reflectance of the land surface. This approach has been applied to GOES Imager and METOP AVHRR data. A similar technique incorporating observations in multiple reflective spectral bands has been implemented in the GOES-R ABI data processing system (Painter et al., 2009). Implementation of the two algorithms with satellite data provides snow fraction estimates comparable both with all current and historic snow fraction products.

The Enterprise Fractional Snow Cover Map Product characterizes the fraction of snow-covered land within the instrument field of view (meaning a sub-pixel snow fraction). It is important that the product does not account for the snow cover that is masked or shadowed by vegetation or topographical features and thus presents the snow fraction which is actually “seen” by the satellite instrument, or the “viewable” snow cover fraction.

The spatial resolution of the product matches the spatial resolution of the sensor data. It equals to 375m for VIIRS, 500m for MetImage and 1-2 km for ABI. Snow fraction is derived only for satellite image pixels over the land surface which are identified by the Binary Snow algorithm as “snow covered”. Given that most clouds are opaque in the visible and infrared spectral range, snow fraction retrievals are performed only in clear sky conditions (no clouds within the instrument field of view). Since the algorithm relies on observations in the reflective bands, daytime conditions are required to estimate the snow fraction. Besides the snow cover fraction map, the product includes a quality flags file which provides support information on the quality of snow retrievals. The Enterprise Binary Snow Map product is delivered in NetCDF format.

1.1.2. Product Requirements

The requirements specified for the VIIRS Fractional Snow Cover product are summarized in Table 1.1. For VIIRS the requirements are provided in GSegDPS (2019). The fractional snow cover is derived in clear sky conditions during daytime (at less than 85 degree solar zenith angle). Retrievals are performed at 375m spatial resolution and should be made at the accuracy of at least 20%.

Table 1-1 – Enterprise Fractional Snow Cover product requirements

Name	Geographic Coverage	Horizontal Res.	Mapping Accuracy	Measurement Range	Measurement Uncertainty	Temporal Coverage Qualifiers	Other Conditions Qualifier
Snow Cover Fraction	Global	VIIRS: 375m MetImage: 500m	1 km	Snow cover fraction (0 - 100%)	20% of the FSC area	Sun at 85 degree solar zenith angle	Clear sky conditions. For pixels identified as snow-covered

.

1.2. Satellite Instrument Description

VIIRS

The Visible Infrared Imaging Radiometer Suite (VIIRS) onboard SNPP and JPSS satellites is a multiband imaging instrument designed to support the acquisition of high-resolution atmospheric imagery and generation of a variety of applied environmental products characterizing the Earth's, atmosphere, oceans, land surface and cryosphere. VIIRS provides spectral observations within 412 nm to 12 μm in 16 bands at moderate spatial resolution of (~750 m at nadir), in a broadband optical moderate resolution day and night band (DNB) and high spatial resolution imagery at ~375 m in nadir in 5 spectral bands centered in the visible, near infrared, shortwave infrared, middle infrared and far infrared spectral range (VIIRS, 2013). As the satellite orbits the Earth, VIIRS scans a swath with the width of about 3040 km. This allows for a complete coverage of the Earth's surface at least two times a day, on ascending and descending node. Observations data are delivered in granules of ~85 seconds long which cover the area of ~3040 by ~570 km in size. The SNPP and JPSS equator crossing time is about 1:30 local time.

MetImage

MetImage is a multispectral (visible and infrared) imaging passive radiometer for METOP SG satellite series. The instrument has 20 spectral bands covering the spectral range from

0.443 to 13.345 μm. It provides across-track scanning of the swath ~2670 km wide with a constant spatial sampling angle across the scan and a spatial resolution of 500m at nadir. Observations from MetIMage will be delivered in the form of granules with the size of granules TBD. The planned launch date for METOP SG A and B satellites is 2023 and 2024 respectively. The equator crossing time for METOP satellites is about 9:30 local time.

ABI

The Advanced Baseline Imager (ABI) is a multispectral radiometer for GOES-R series satellites providing observations of the reflected and emitted radiation with 16 bands within a broad spectral range from visible to thermal infrared. The coverage of ABI instrument onboard GOES-East and GOES-West satellite is limited to the Western Hemisphere. The spatial resolution in nadir is 0.5 km in the visible spectral, 1 km in other reflective bands and 2 km in infrared bands. The instrument has multiple scan modes allowing for image updates at up to 30 sec time interval.

2. ALGORITHM DESCRIPTION

This section presents the detailed description of the algorithms to generate the Fractional Snow Cover product.

2.1. Processing Outline

The Enterprise Fractional Snow Cover algorithms and products provide estimates of the snow cover fraction as seen by the satellite instrument ("viewable snow fraction). The derived snow fraction does not account for the snow cover masked by the forest canopy and is therefore different from the true fraction of the snow cover on the ground.

The primary input to the algorithm consists in the Binary Snow Cover Map product, the observed spectral reflectance in the visible and in the shortwave infrared spectral band and information on the viewing and illumination geometry of observation. The snow fraction retrieval algorithm is applied on a pixel-by-pixel basis to pixels labeled as "snow covered" by the Binary Snow Cover Map. Cloudy pixels and water pixels as identified in the quality flags of the Binary Snow Cover Map are excluded from the retrievals.

Both snow fraction algorithms are one-step algorithms utilizing a linear unmixture approach with two end-members corresponding to snow free and completely snow covered land surface. The MODIS-heritage NDSI-based snow fraction converts NDSI into the snow fraction using a linear relationship with fixed slope and intercept parameters. The latter is equivalent to an implicit assumption of fixed end-member values. The reflectance-based algorithm also assumes fixed values for the snow-free and fully snow-covered land surface however these values are corrected for changing satellite-solar geometry of observations.

2.2. Algorithm Input

The Fractional Snow Cover algorithm input includes sensor and ancillary input data. The ancillary data include both satellite-derived data and static datasets.

Table 2-1 provides information on the primary sensor input to the algorithm. At this time as the input the algorithm uses satellite observations in the visible and shortwave infrared spectral bands. In the future modifications of the algorithm involving the near-infrared (I2) and middle infrared spectral band data (I4) are assumed. Additional sensor input data include Latitude, Longitude of the pixel along with the observation geometry characterized by the Solar Zenith Angle, Satellite View Angle and Solar-Satellite Relative Azimuth. Observation geometry angles are specified for each satellite pixel.

Table 2-1 – Primary sensor input to Enterprise Fractional Snow Cover algorithm

Spectral Band	VIIRS Band (resolution, m)	VIIRS Central Wavelength (μm)	MetImage Band (resolution, m)	MetImage Central Wavelength(μm)	Input Type
Visible	I1(375m)	0.640	VII-12 (500m)	0.668	Current
Shortwave IR	I3(375m)	1.61	VI-24 (500m)	1.63	Current

Besides the sensor inputs, the Fractional Snow Cover algorithm uses the Binary Snow Cover map as an input. Properties of the derived products used by the Fractional Snow Cover Maps are provided in Table 2-2.

Table 2-2 – Derived satellite products used by the Fractional Snow Cover algorithm

Name	Description	Dimension
Binary Snow Cover	Binary (snow/no-snow) map	Granule

Input static datasets include coefficients defining the relationship between the NDSI and snow fraction for the NDSI-based snow fraction algorithms and coefficients defining the BRDF model for snow and for the snow –free land surface. The list of Input static data sets and their description is given in Table 2-3

Table 2-3 – Input static datasets used by the Fractional Snow Cover algorithm

Name	Description	Dimension
NDSI-based Snow Fraction model parameters	Two coefficients defining the linear relationship between NDSI and Snow Fraction	2
Reflectance-based Snow Fraction model parameters	Kernel loads for the snow and snow-free land surface kernel-driven BRDF models	(2,8)

2.3. Theoretical Description

Estimation of a sub-pixel snow cover faction is based on a strong difference between the spectral reflectance of snow and of the snow-free land surface. In the visible to near-infrared spectral range (0.6 -0.9 μm) snow cover increases the land surface reflectance from 0.05 to 0.4 typical for bare soils and snow-free vegetated surfaces to up to 0.8- 0.9 corresponding to the reflectance of the pure snow. In the shortwave infrared (at wavelengths longer than 1.6μm) the snow reflectance is smaller than the reflectance of most land surface cover types (see Figure 2-1). These differences allow not only for identification of the snow cover within the instrument field of view but also for estimating the fraction of the instrument footprint covered with snow or the fractional snow cover.

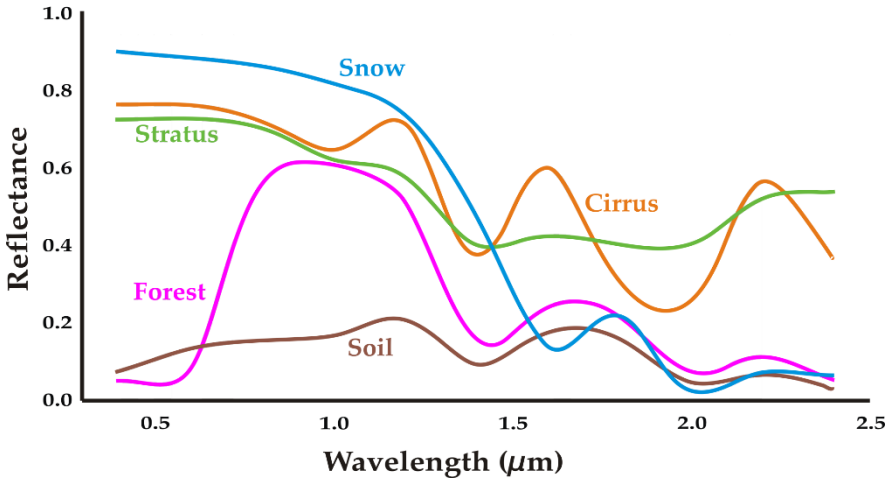

Figure 2-1– Spectral reflectance of natural surfaces and clouds

In the existing snow fraction retrieval algorithms the snow fraction within the image pixel is estimated within a linear mixture approach. In this approach the spectral response of a "mixed" pixel is represented as the sum of responses of every land cover type or end-member, weighted by their respective area proportion in the instrument field of view. The primary difference between various snow fraction retrieval techniques concerns the selection of the spectral bands and particular spectral features used in the retrievals along with the selection of end-members and approaches to establish their spectral features.

The majority of developed snow fraction algorithms relate the subpixel snow fraction to the observed reflectance of the scene. Rosenthal and Dozier (1996) derived the snow fraction from Landsat TM-observed reflectance with an unsupervised linear unmixing technique and end-members determined from the image data. Manually selected end-members including multiple end-members representing snow cover with different grain size were utilized by Nolin et al. (1993) to analyze “mixed” pixels in the imagery acquired with the Airborne Visible/Infrared Imaging Spectrometer (AVIRIS). Vikhamar and Solberg (2003) developed a method to retrieve the snow fraction over a forested area. In this work the reflectance spectra of end-members (snow cover and different forest cover types) was determined using a physically based model along with the results of in situ surface reflectance measurements. Painter et al (2009) developed a multispectral multi-end-member snow fraction algorithm which was tested with MODIS data. As input the algorithm needs atmospherically corrected normalized reflectance values. A similar algorithm has been proposed for and incorporated in the GOES-R ABI data processing system. A less sophisticated one-band algorithm has been developed in Romanov et al (2003) and applied to GOES Imager data. The latter technique uses observations in the visible spectral band and two end-members representing completely snow covered and snow free land surface. The algorithm incorporates a kernel-driven BRDF model correcting the end-member reflectance for changing the view and illumination geometry of observations.

In several studies rather than the reflectance the snow fraction is assumed proportional to the value of the Normalized Difference Snow index (NDSI). Barton et al. (2000) applied this approach to Landsat TM data. A similar technique was developed by Appel and Salomonson (2002) for the Moderate Resolution Imaging Spectroradiometer (MODIS) on board EOS satellites. In the latter study the statistical relationship between the snow fraction and NDSI was established through comparing MODIS scenes with co-registered classified images from Landsat TM. The NDSI-based snow fraction product was part of NASA MODIS set of cryosphere products since early 2000s up until Collection 6.

All algorithms listed above estimate the viewable snow fraction, which characterizes the fraction of snow cover within the instrument footprint which is “seen” by the sensor. A more challenging approach of Metsämäki e al (2005) accounts for the masking effect of the forest canopy and infers the true snow cover fraction on the ground. Application of this technique however requires an accurate characterization of the forest cover transmissivity which is not readily available and which may be changing with the season.

Due to the use of different spectral bands and different spectral features in the existing algorithms estimates of the snow fraction may be substantially different. In particular large differences between the NDSI-based snow fraction and reflectance-based snow fraction derived from MODIS data have been reported by Ritger et al., (2013). Later Riggs and Hall (2015) determined that the NDSI-based algorithm quickly “saturates” at high NDSI values and prevents from proper characterization of the snow fraction when NDSI exceeds 0.7.

Due to this fact the production of NDSI-based snow fraction product with MODIS data was terminated. Although the NDSI-based snow fraction product is not optimal for characterizing the snow fraction on the ground, there are users that still prefer to uses this approach. Therefore in the current version of the Enterprise snow products we decided to keep both snow products, the reflectance-based and the NDSI-based.

2.3.1. Physical Description

Reflectance-based Snow Fraction

The Enterprise reflectance-based snow fraction algorithm inherits the principal approach to the snow fraction estimate incorporated in the snow fraction algorithm developed earlier for GOES Imager data (Romanov et al., 2003). It uses observations in the visible spectral band centered at around 0.6μm and applies a linear unmixing technique to determine the snow-covered portion of a scene within the instrument field of view. The two end-members incorporated in the algorithm represent correspondingly a completely snow covered and completely snow free land surface.

$$SnowFractionRefl=(R-R_{land})/(R_{snow}-R_{land}), \quad (1)$$

Where R is the observed visible reflectance of the scene, R_{snow} and R_{land} are the visible reflectance of end-members representing the snow-free and the snow-covered land surface, respectively.

It is important that the reflectance of both end-members exhibits a strong angular anisotropy which has to be accounted for when inferring the snow fraction from satellite data. We adopted an empirical approach to determine R_{land} and R_{snow} along with the reflectance anisotropy inherent to the snow-free and snow-covered land surface. For the VIIRS snow fraction algorithm the reflective properties of a completely snow-covered land surface were established from observations over ice fields in Central Greenland, whereas bidirectional reflectance of snow-free land was determined from the analysis of summer-time observations over North America middle and high latitude area (see Fig 2-2 for the location of the two regions).

To establish the end-member reflectance values VIIRS SNPP clear sky observations in the visible spectral band were collected during two six months periods from March 2013 to September 2013 and from March 2014 to September 2014. Pixels identified as “snow-covered in the VIIRS Binary Snow cover maps product were excluded from the snow-free land dataset. When determining the reflectance of the snow-free land surface no distinction was made between surfaces with different vegetation cover type.

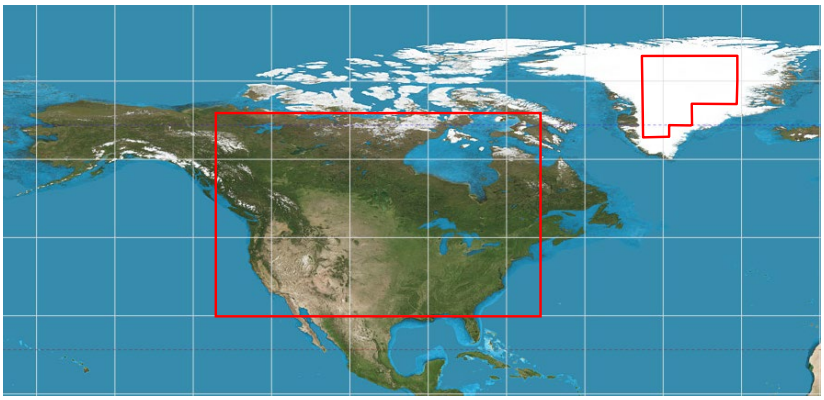

Figure 2-2– Geographical regions where VIIRS observations were collected to characterize the reflectance of snow-free and snow covered land surface

The analysis of VIIRS SNPP observation geometries has shown that in the middle and high latitudes observations are performed far away from the principal plane geometry with the solar-satellite relative azimuth ranging within 60 to 120 deg. Since for natural land surface cover types reflectance does not change much with changing relative azimuth when observations are made across the principle plane geometry, azimuthal variations of snow and land reflectance were disregarded and the observed reflectances were averaged across all relative azimuth angles. Graphs in Figure 2-3 illustrate changes of the observed snow and snow-free land reflectance with solar and satellite zenith angle.

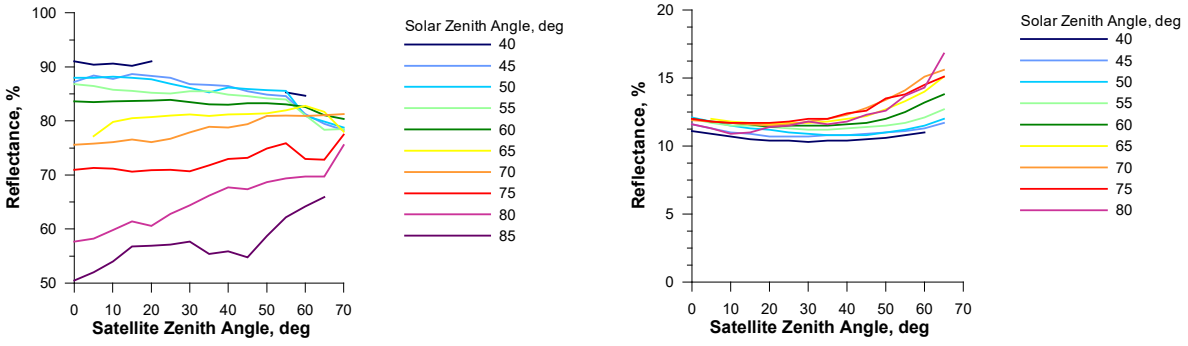

Figure 2-3– Satellite-observed visible (band 1) reflectance of snow cover (left) and snow-free land surface (right) as a function of the solar and satellite zenith angle. Observations included in the statistics were made across the principle plane at the solar-satellite relative azimuth angle within 60 deg to 120 deg.

To reproduce the reflectance anisotropy of snow and snow-free land surface in the snow fraction retrieval algorithm we have tested several kernel-driven models incorporating different combinations of trigonometrical functions of the solar and satellite zenith angles. The intent was to establish the model yielding the closest fit to the observed reflectance at all angles with the least number of kernel functions used. The following 8-term parameterization was found to most optimally satisfy the objective:

$$R = C_0 + \Sigma_{i=1,7} C_i F_i \quad (2)$$

where $F_1 \ldots F_7$ are kernel functions having the form $F_1 = \cos(\theta_{sol})$, $F_2 = \cos(\theta_{sat})$, $F_3 = \cos(\theta_{sol}) \cos(\theta_{sat})$, $F_4 = \cos^2(\theta_{sol})$, $F_5 = \cos^2(\theta_{sat})$, $F_6 = \cos^4(\theta_{sol})$, $F_7 = \cos^4(\theta_{sat})$ and $C_0 \ldots C_7$ are corresponding kernel loads. The kernel loads were estimated within a simple least-square approach and are given in Table 2-4. Graphs illustrating the reflectance anisotropy of snow cover and snow-free land provided by the developed model are given in Figure 2-3.

Table 2-4 – Kernel functions and corresponding kernel loads for the reflectance anisotropy model of snow cover and snow-free land surface.

Kernel Functions	Kernel Loads	Kernel Load Values	
		Snow-free land	Snow
1.	C_0	19.02	63.45
$\cos(\theta_{sol})$	C_1	9.699	89.90
$\cos(\theta_{sat})$	C_2	-9.944	-16.33
$\cos(\theta_{sol}) \cos(\theta_{sat})$	C_3	13.16	61.81
$\cos^2(\theta_{sol})$	C_4	-36.30	-140.9
$\cos^2(\theta_{sat})$	C_5	-6.289	-5.114
$\cos^4(\theta_{sol})$	C_6	20.18	51.62
$\cos^4(\theta_{sat})$	C_7	5.419	-2.623

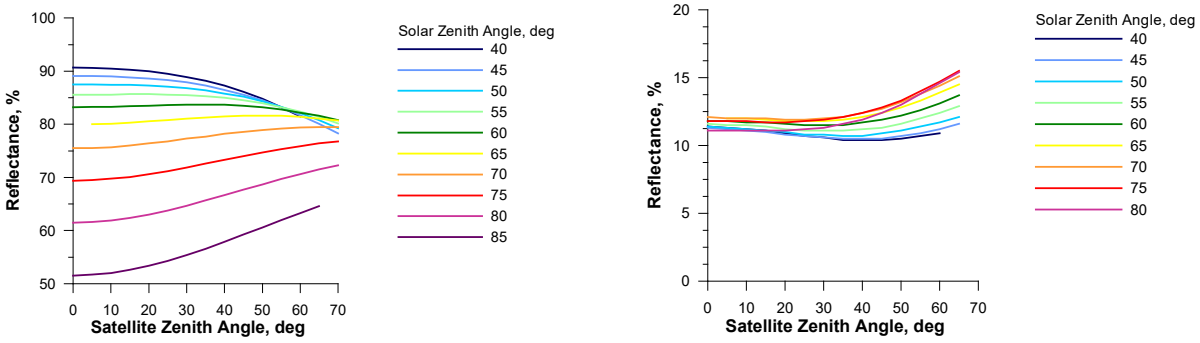

Figure 2-3– Top of the atmosphere visible reflectance of snow cover (left) and snow-free land surface (right) as a function of solar and satellite zenith angle simulated with the developed kernel-driven model.

Application of the developed BRDF model substantially reduces variation inherent to the observed visible reflectance of snow and of the snow-free land due to the reflectance anisotropy. In particular variation of about 40% inherent to the original top of the atmosphere snow reflectance and of about 7% in the observed reflectance of the snow-free land surface decreases correspondingly to 6-7% and 2% in the anisotropy-corrected reflectances.

The kernel loads of the reflectance anisotropy model for snow and for the snow-free land surface are designed to be tunable parameters that maybe updated as a result of prelaunch tuning and on-orbit calibration and validation.

NDSI-based Snow Fraction

The Normalized Difference Snow Index (NDSI) is widely used to identify snow cover in the field of view of satellite radiometers. NDSI is a spectral index expressed as

$$NDSI=(R_{vis} - R_{swir}) / (R_{vis} + R_{swir}) , \quad (3)$$

where R_{vis} and R_{swir} are the observed reflectances in the visible (VIIRS band I1) and in the shortwave infrared (VIIRS band I3) spectral band.

Salomonson and Appel (2003) compared MODIS-based NDSI with the higher spatial resolution snow retrievals with Landsat data and established that the snow fraction is related to NDSI. Figure 2-4 presents several example of NDSI and snow fraction scatter plots for a number of scenes reproduced from the paper cited above.

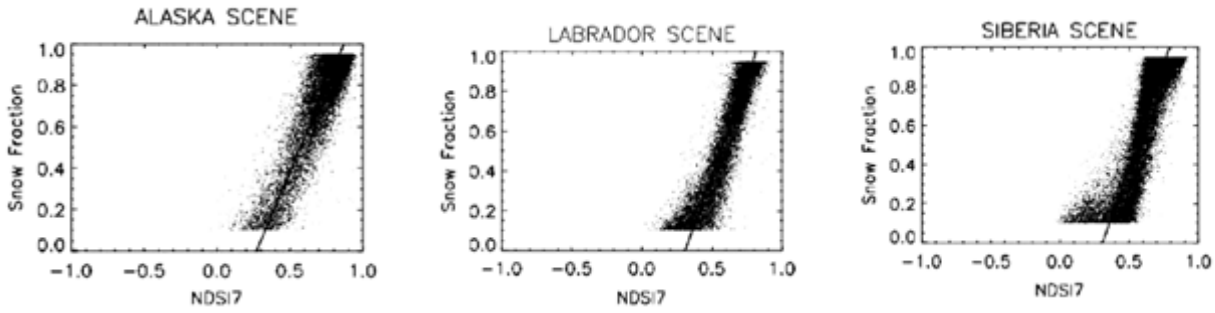

Figure 2-4– Landsat snow fraction and matching MODIS NDSI scatter plots reproduced from Salomonson and Appel (2003) .

It was proposed to use approximate the relationship with a linear function of the form

$$SnowFractionNDSI = a + b * NDSI, \quad (4)$$

Where ***NDSI*** is the satellite-observed NDSI value

The best match between the snow fraction and NDSI was achieved with a=-0.01 and b=1.45.

The NDSI-based snow fraction formula is equivalent to a linear unmixture algorithm

$$SnowFractionNDSI = (NDSI - NDSI_{land}) / (NDSI_{snow} - NDSI_{land}), \quad (5)$$

where $NDSI_{land}$ = 0.007 and $NDSI_{snow}$ = 0.70

For VIIRS the value of NDSI is calculated from observations in bands I1 centered at in the visible spectral range at 0.6 μm and I3 centered in the shortwave infrared spectral range at around 1.6 μm.

The NASA MODIS team has tested the MODIS snow fraction algorithm with VIIRS data and found that the optimal values of ***a*** and ***b*** for VIIRS were the same as for MODIS (G.Riggs, personal communication).

The slope and intercept coefficients ***a*** and ***b*** in Formula (4) are designed to be tunable parameters that maybe updated as a result of prelaunch tuning and on-orbit calibration and validation.

Planned modifications for the MetImage and ABI snow fraction algorithm

Fractional snow cover is part of cryosphere products to be derived from METOP SG MetImage data and observations from ABI onboard GOES-R series satellites. Considering known deficiencies of the NDSI-based snow fraction product we may follow the MODIS team and abandon this snow cover algorithm and product. As a result, snow fraction from MetImage and ABI data will be derived solely with the reflectance-based snow fraction algorithm.

Given that the current snow fraction algorithm has been developed for VIIRS and that spectral bands of METImage and ABI are somewhat different from corresponding bands of VIIRS (see Table 2-1) we expect that modification to the original algorithm may be needed. These modifications will concern primarily the endmembers incorporated in the algorithm, i.e., the values of the snow-free land and of snow cover reflectance and BRDF models characterizing their change with the observation geometry. Since the observation geometry of MetImage is similar to VIIRS, modifications may be limited to the values of kernel weights incorporated in the BRDF model (Formula 2) that would account for a possible difference in the spectral response function of the visible band of VIIRS and MetImage. Adjusting the existing algorithm for ABI appears more challenging because of its different observation geometry. It may require reformulation of the BRDF model to optimally reproduce the reflectance angular anisotropy in the backscatter hemisphere.

Since updating the coefficients for the BRDF model require a substantial amount of accumulated observations, we do not expect modifications to be ready, tested and introduced to the METImage Snow Fraction algorithm before the operational data become available. Up until this time the VIIRS BRDF model will be used with MetImage. Development and testing of BRDF models for ABI are currently scheduled for the second half of 2020- beginning of 2021. Operational Implementation of these updates may occur in the middle of 2021.

2.3.2. Mathematical Description

Implemented algorithms follow their description provided in Section 2.3.1 and are applied on a pixel-b pixel basis. Once the pixel is confirmed as “clear sky” and “snow covered”, the snow fraction is estimated. For VIIRS two snow fraction algorithms (reflectance-based and NDSI-based) are applied sequentially. For subsequent implementations only the reflectance based snow fraction will be derived.

The reflectance-based algorithm calculates the reflectance of end-members adjusted for the given observation geometry using Formula (2) and then applies Formula (1) to determine the fractional snow cover.

The NDSI-based algorithm uses VIIRS observations in bands I1 and I3 to calculate the value of NDSI using Formula (3) and then applies Formula (4) to determine the fractional snow cover within the instrument field of view.

2.4. Algorithm Output

The VIIRS algorithm output includes the two fractional snow cover maps derived within the reflectance-based and NDSI-based approaches, the quality flags associated with the maps and metadata. For a detailed description of the algorithm output see Tables 2-5 and 2-6. The fractional snow cover maps and the quality flags present the arrays of the size corresponding to the size of the VIIRS granule. Metadata is a text file. The output is provided in NetCDF format. The Snow Fraction product derived from observations of MetImage and ABI will incorporate only one parameter, the reflectance-based snow fraction.

Figure 2-5 gives an example of granules of the two VIIRS snow fraction products. Figure 2-6 provides an example of a daily global snow fraction map generated from all snow fraction granules produced in the course of one day.

VIIRS granule: 20131111_1933578

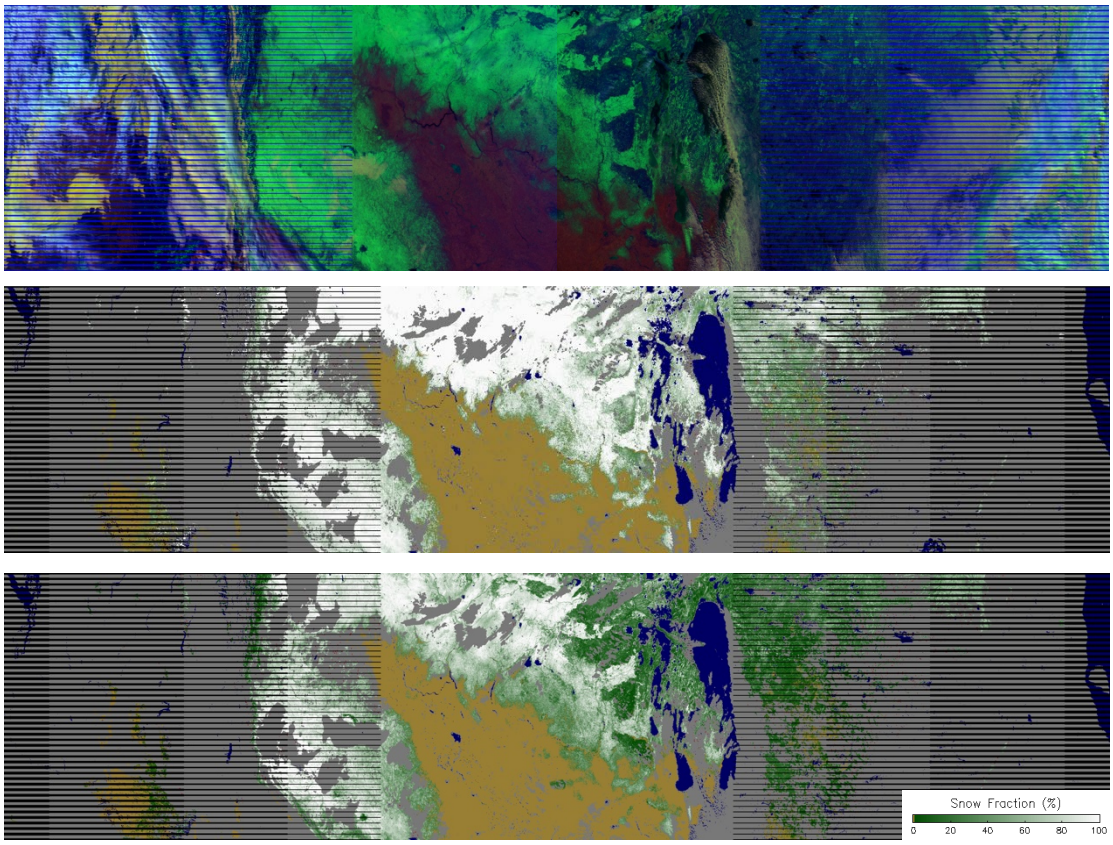

Figure 2-5– Example of VIIRS granule false color images (upper), NDSI-based snow cover fraction (middle) and reflectance-based snow cover fraction (lower). November 11, 2013

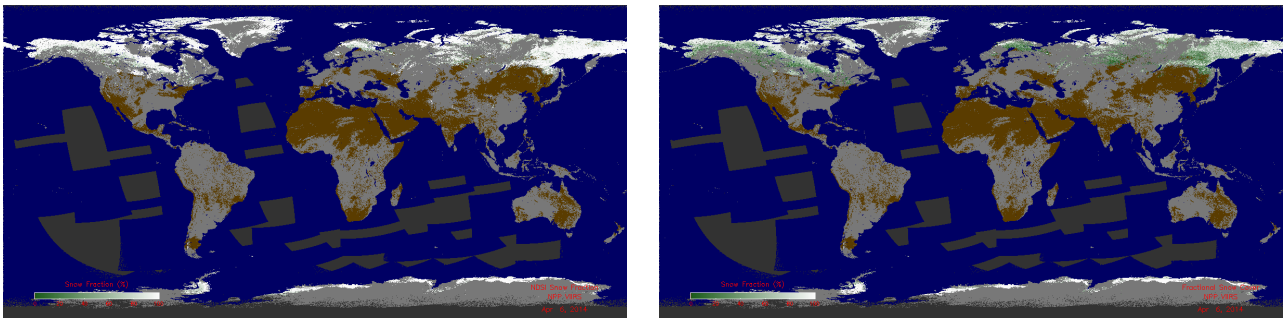

Figure 2-6– Example of global gridded maps of NDSI-based snow fraction (left) and reflectance-based snow fraction (right) .

Table 2-5 Fractional Snow Map output parameters (1 byte)

Parameter	***Description***	***Unit***
Fractional Snow Cover NDSI-based (VIIRS only)	Reports the area fraction of pixel covered by snow as seen by satellite sensor ("viewable snow fraction") Value 0: No snow on the ground 1: 1% snow fraction 2: 2% snow fraction . . . 100: 100% snow fraction 128: No retrieval	Percent
Fractional Snow Cover Reflectance-based	Reports the area fraction of pixel covered by snow as seen by satellite sensor ("viewable snow fraction") Value 0: No snow on the ground 1: 1% snow fraction 2: 2% snow fraction . . . 100: 100% snow fraction 128: No retrieval	Percent

Table 2-6 Snow Map Quality Information (1 byte)

Parameter	***Description***	***Unit***
Quality Flag	Provides product quality information Value 0 : Good retrieval 105: water 110: cloud 111: rejected snow due to inconsistency with snow climatology 112: rejected snow, inconsistent with surface temperature climatology 113: rejected snow, failed spatial consistency test	Unitless

	114: rejected snow, failed temperature uniformity test 121: night, insufficient solar illumination 122: undetermined 124: bad pixel SDR 125: fill value 128: No retrieval	

2.5. Performance Estimates

2.5.1. Test Data Description

The Snow fraction algorithms have been tested and validated using global VIIRS observations collected from both SNPP and NOAA-20 satellites during different seasons of the year.

2.5.2. Sensor Effects

Any sub-optimal performance of the VIIRS sensors may cause degradation of the quality of the VIIRS snow fraction retrievals. This concerns, first the VIIRS sensors in bands I1 and I3 which are directly used to estimate the fractional snow cover. It is important that the Enterprise fractional snow cover product uses the Enterprise binary snow cover product whereas the latter incorporates the cloud mask provided in the Cloud Mask product. Therefore, the excessive noise or inadequate calibration of sensors involved in the production of these two input products may adversely affect the accuracy of the Enterprise Fractional Snow Cover Map product.

Some geophysical phenomena causing a substantially reduced atmospheric transmittance in the visible and in the shortwave infrared band (e.g., smoke from fires or dust from volcanic eruptions) will also adversely affect snow fraction retrievals. These phenomena can cause underestimate of the snow fraction as well as its overestimate depending on a particular scene, the fraction of snow on the ground and observations geometry.

2.5.3. Retrieval Errors

Direct quantitative estimation of the accuracy of satellite-based snow fraction retrievals is hardly possible. The snow fraction is a remotely sensed radiance-based parameter and observations of the snow fraction are not routinely performed on the ground. Visual

estimates of the fraction of the ground surface are sometime included in snow surveys, but these measurements are performed at 10-, 14- days or one month time interval mostly during the snow melt period at selected meteorological stations. They are not included in standard SYNOP-FM12 WMO reports and are not transmitted through GTS. Moreover the snow fraction observed in situ is a true fraction of the land covered with snow and is thus principally different from the satellite-based viewable snow fraction which excludes snow cover masked by the vegetation. Therefore, only theoretical estimates of retrieval errors are possible.

Theoretical error budget

Theoretically errors in the estimated reflectance-based snow cover fraction are determined by uncertainty in the observed and predicted top of the atmosphere (TOA) reflectance in the right side of equation (1). For the NDSI-based snow fraction estimation errors are, first due to uncertainty in the observed NDSI values and, second due to variable end-members NDSI values in Equation (5). Uncertainty in the NDSI value is determined by corresponding reflectance uncertainties in bands 1 and 3. Detailed theoretical error budget for the two snow fraction estimates is given in Tables 2-7 and 2-8.

In the estimates presented in Tables 2-7 and 2-8 it was assumed that the uncertainty in the observed reflectance is due to the calibration uncertainty and variable atmospheric transmittance. The uncertainty of the visible reflectance of snow and snow-free land surface in the reflectance-based snow fraction included the effect of the natural spatial variability of the land surface reflectance and residual errors of the reflectance anisotropical correction. Since the NDSI-based snow fraction algorithm implicitly assumes fixed NDSI values for the snow-free land surface and for snow, the snow fraction retrieval errors incorporate the effect of both natural variability of the reflectances of snow and of the snow-free land and the reflectance anisotropy inherent to these surface cover types in both visible and shortwave infrared spectral bands.

As it follows from Table 2-8 the largest contribution to the uncertainty of the NDSI-based snow fraction results from the uncertainty in the reflective properties of the snow-free land surface. It causes corresponding uncertainty of up to 0.35 in the NDSI of the snow-free land surface. It should be noted that overall uncertainty levels the NDSI-based snow fraction may be overestimated since in the calculations we assumed that variations in the visible and shortwave infrared reflectance are independent, whereas in fact these values may be related.

Table 2-7- Factors contributing to the uncertainty of the derived reflectance-based snow fraction.

Factor	Affected Reflectance	Assumed uncertainty	Estimated uncertainty in the derived snow fraction
Visible reflectance measurement noise and calibration error	Observed Band I1 reflectance	0.005	0.006
Variable atmospheric composition	Observed Band I1 reflectance	0.1	0.11
Variable reflective properties of the snow-free land surface in band I1	Snow-free land visible reflectance ($\mathbf{R_{land}}$)	0.1	0 to 0.11
Variable reflective properties of snow	Snow visible reflectance ($\mathbf{R_{snow}}$)	0.05	0 to 0.06
Residual uncertainty of snow reflectance due to angular anisotropy	Snow visible reflectance ($\mathbf{R_{snow}}$)	0.03	0 to 0.04
Residual uncertainty of snow-free land reflectance due to angular anisotropy	Snow-free land visible reflectance ($\mathbf{R_{land}}$)	0.03	0 to 0.04
All factors combined			0.15 to 0.20

Table 2-8 - Factors contributing to the NDSI-based snow fraction uncertainty

Factor	Affected reflectance	Assumed uncertainty	Affected NDSI parameter	Estimated effect on NDSI	Estimated uncertainty in the derived NDSI-based snow fraction
Visible reflectance measurement noise and calibration error	Observed reflectance in the visible band	0.005	Observed **NDSI**	0.0005 to 0.02	0 to 0.03
Shortwave Infrared reflectance measurement noise and calibration error	Observed reflectance in the shortwave infrared band	0.005	Observed **NDSI**	0.0005 to 0.02	0 to 0.03
Variable atmospheric composition	Observed reflectance in the visible band	0.05	**Observed NDSI**	0.005 to 0.2	0.01 to 0.3

Variable atmospheric composition	Observed reflectance in the shortwave infrared band	0.01	Observed **NDSI**	0.02 to 0.05	0.03 to 0.07
Variable reflective properties of the snow-free land surface in band I1 (spatial and angular)	Snow-free land visible reflectance ($\mathbf{R_{land}}$)	0.08	$\mathbf{NDSI_{land}}$	0.20 to 0.23	0.27 to 0.35
Variable reflective properties of snow in band I1 (spatial and angular)	Snow visible reflectance ($\mathbf{R_{snow}}$)	0.1	$\mathbf{NDSI_{snow}}$	0.01	0.01
Variable reflective properties of the snow-free land surface in band I3 (spatial and angular)	Snow-free land shortwave infrared reflectance ($\mathbf{R_{land}}$)	0.08	$\mathbf{NDSI_{land}}$	0.11 to 0.23	0.17 to 0.35
Variable reflective properties of snow in band I3 (spatial and angular)	Snow shortwave infrared reflectance ($\mathbf{R_{snow}}$)	0.05	$\mathbf{NDSI_{snow}}$	0.1	0.12
All factors combined					0.33 to 0.40

2.6. Practical Considerations

2.6.1. Numerical Computation Considerations

Both snow fraction algorithms are simple from the mathematical stand point . They are not computationally intensive as they do not involve iterations complex physical models or inversion of large matrices. Both algorithms are applied on a pixel by pixel basis and do not require the analysis of a spatial structure of the spectral response of larger scenes.

2.6.2. Programming and Procedural Considerations

None

2.6.3. Quality Assessment and Diagnostics

The quality of the satellite-based snow fraction retrievals will be estimated two ways, first through a series of consistency test and, second through comparison of sub-pixel snow fraction retrievals with snow fraction derived from higher spatial resolution satellite data

Consistency Tests

To indirectly assess the validity of the snow fraction product we evaluate the realism of spatio-temporal variations of the derived snow fraction and examine the product consistency with other satellite observations and independent environmental datasets. Several tests are applied to assess consistency of the derived snow cover fraction. The derived snow fraction is examined for self-consistency and is compared with the forest cover distribution and snow depth observations.

Temporal changes of the fractional snow cover occur predominantly due to snow-falls and to the snow melt. Without these events the spatial pattern of the snow fraction should not much from one day to another. Within the self-consistency test we compare snow fraction products on two consecutive days and examine correlation and the absolute difference between the retrieved values. We also compare snow fraction retrievals at a different time lag. It is expected that the day-to-day autocorrelation of the snow fraction retrievals should be strongly positive, above 0.5 and the differences in the derived snow fraction values should generally be within the specified accuracy requirements for the snow fraction. Correlation is expected to decrease with the increasing time lag.

Forests present the major factor controlling the spatial distribution of the viewable snow fraction. Masking of snow cover on the forest floor by the vegetation canopy causes a substantial reduction in the viewable snow fraction. Within this test we compare the derived daily snow fraction with available information on the forest cover distribution. It is expected that the snow fraction should exhibit a strongly negative correlation with the forest cover fraction. An example of time series of daily correlation between the fractional snow cover and the forest cover fraction for two snow fraction products is given in Figure 2-7. Our analysis shows that the reflectance-based snow fraction exhibits a stronger negative correlation with the forest fraction than the snow fraction derived with the NDSI-based algorithm.

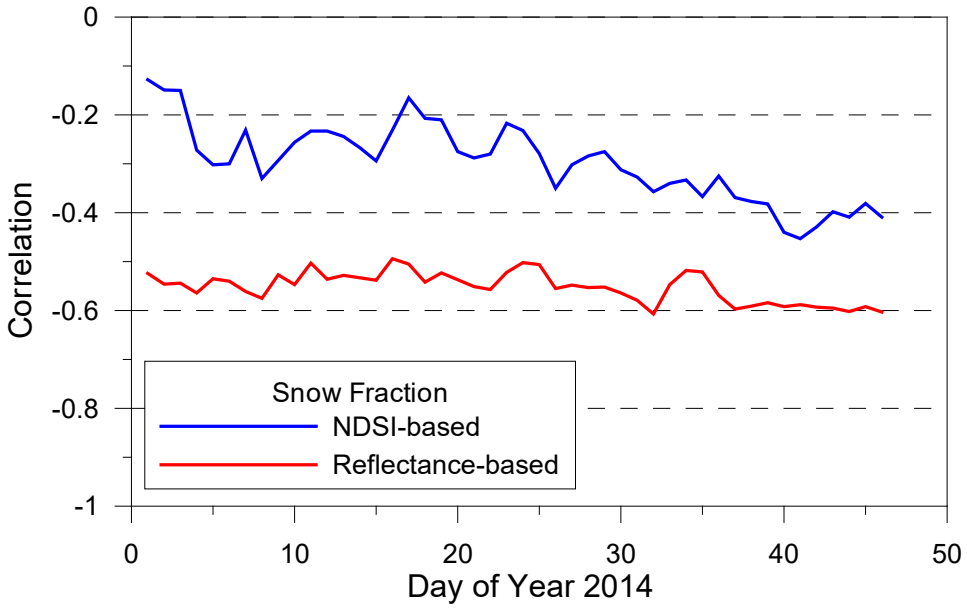

Figure 2-7– Time series of correlation between the snow fraction and forest fraction distribution for two snow fraction products, NDSI-based and reflectance-based.

Over flat non-forested areas the primary factor determining the viewable snow fraction is the snow depth. Therefore, the derived snow fraction should increase with increasing snow depth and vice versa. Within this test we match satellite-derived snow fraction retrievals and the results of snow depth observed in situ. It is expected that the correlation between the two parameters should be positive. Lack of correlation or negative correlations may be indicative of the problems in the algorithm or the input data. For the analysis we use observations over US Great Plains and Canadian prairies.

Figure 2-8 presents time series of daily correlation between the snow depth and the snow fraction for two snow fraction products in January and February 2014. The correlation of the two products with the snow depth is not very strong but still positive ranging from 0.1 to 0.6.

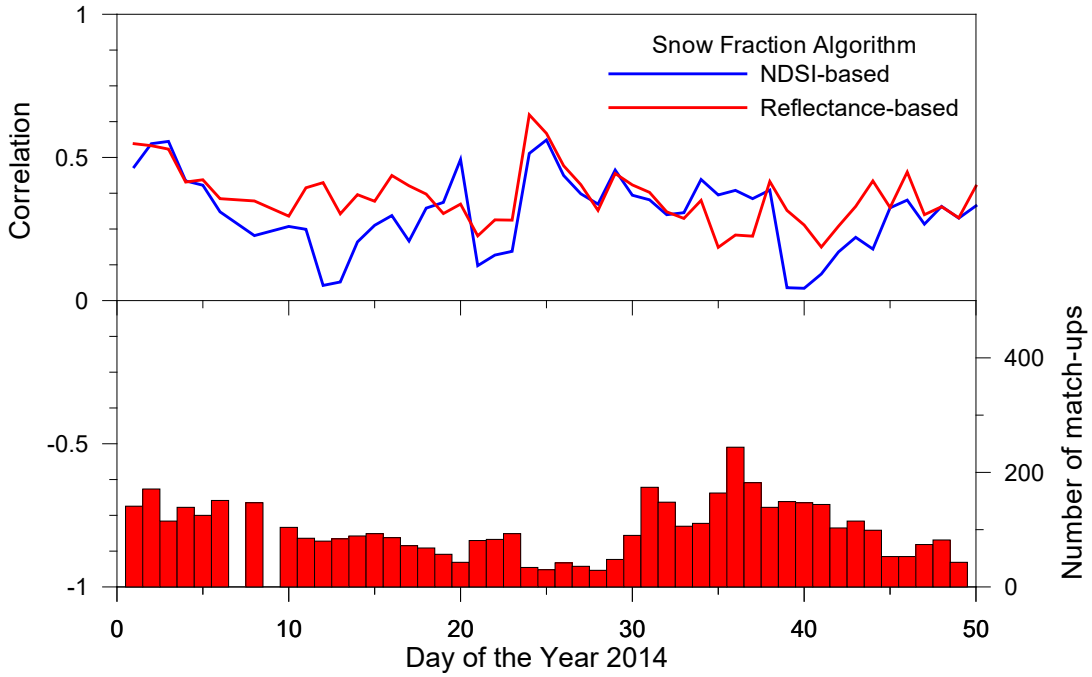

Figure 2-8– Time series of correlation between the snow fraction and in situ observed snow depth over US Great Plains and Canadian Prairies in January and February 2014.

Comparison of snow fraction derived from different satellite platforms

Comparison of reflectance-based snow fraction retrievals from VIIRS observations onboard SNPP and NOAA-20 satellites has demonstrated their agreement to within about 0.1. An example of the comparison of matched observations from SNPP and NOAA-20 is presented in Figure 2-9.

One of the primary factors determining the accuracy of snow fraction retrievals consists in the accuracy of parameterization of the reflectance anisotropy of the snow-free land surface reflectance and of the snow cover. Due to a small difference in the overpass time spatially matched VIIRS observations from SNPP and NOAA-20 are practically synchronous, however the observation geometry associated with these observations (e.g., satellite zenith angle and solar-satellite relative azimuth) are different. Close agreement on the value of the snow fraction, estimated from observations taken at different geometry suggests a high accuracy of the applied models of surface reflectance anisotropy.

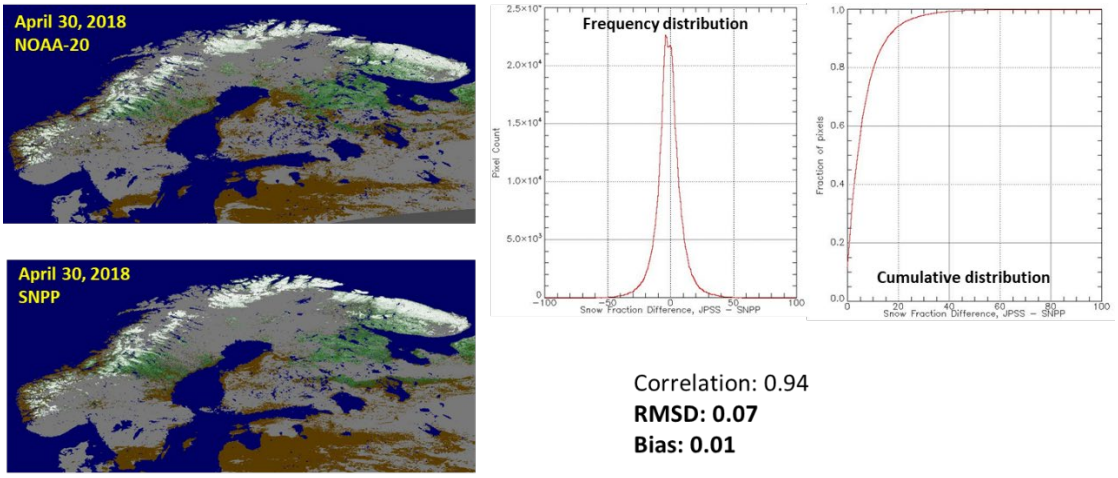

Figure 2-9– Comparison of snow fraction derived from VIIRS observations onboard SNPP and NOAA-20 satellites.

Comparison with finer spatial resolution satellite observations

In a number of studies a surrogate approach to validate the satellite derived snow fraction has been applied where the snow fraction within the satellite field of view was estimated from finer spatial resolution observations with another but similar satellite sensor. In particular, Salomonson and Appel (2004), Painter eta l (2009) and Rittger (2013) used binary snow retrievals with Landsat TM observations to validate the snow fraction derived from MODIS data. The weakness of this approach however results from the fact that both sensors have similar spectral bands which are used for snow identification and that snow identification with both sensors data is typically performed with the same algorithm. Moreover, the principal assumption of this approach that there are no “mixed” or partially snow-covered pixels at the fine spatial resolution can hardly be ever satisfied unless the coarser resolution grid cell is completely snow-free of completely snow-covered.

The results of the quality assessment will be documented and posted at a dedicated web site. Anomalies of the product performance will be timely identified, reported, analyzed and conclusions of the source of anomalies and possible remedies will be made.
.

2.6.4. Exception Handling

The developed software is designed to handle a wide variety of processing problems, including bad and missing data and fatal errors. In the event that processing problems

prevent the production of useful snow fraction retrievals, error flag will be written to the output product file as metadata.

2.7. Validation

Validation of the algorithm and of the VIIRS product will be performed according to the schedule proposed in the Calibration/Validation Plan for Fractional Snow Cover Product (JPSS, 2015) and will include the following Beta, Provisional and Validated maturity levels. A similar approach will be taken when validating the snow fraction from MetImage and ABI

3. ASSUMPTIONS AND LIMITATIONS

3.1. Performance Assumptions

It is assumed that cloud masking and snow cover identification is accurate. Pixels erroneously identified as snow covered by the binary snow cover algorithm will be assigned a non-zero snow fraction value.

The two algorithms incorporated in the snow fraction product utilize principally different assumptions with respect to the relationship of the snow fraction to the spectral response of the scene. The reflectance-based algorithm assumes that the snow fraction is linearly related to the visible reflectance. This assumption is physically natural, it is implicitly used when visually estimating the fractional snow cover over the land surface and is also applied in a large number of land surface models.

The NDSI-based algorithm assumes a linear relationship of the NDSI to the snow fraction. The validity of this latter assumption is less obvious from the physical stand point. Although the NDSI index is sensitive to the presence of snow, the established linear relationship between the snow fraction and NDSI is based on the correlative analysis of two satellite datasets at two different spatial resolution and does not involve any in situ measurements or observations.

There are other assumptions in both algorithms generating the snow fraction products. Some of them an inherent to both algorithms and some are algorithm specific.

The two algorithms implement a two-endmemeber one band linear unmixture technique to derive the snow fraction. The end-members characterize a completely snow-free and completely snow-covered land surface. In both cases the snow-free land surface end-member does not account for possible variability of reflective properties of the land surface due to different land cover types. Possible variability in the reflective properties of snow is

also not accounted for. While the reflectance-based algorithm corrects the reflectances for the angular anisotropy, the NDSI-based algorithm assumes NDSI independent on the observation geometry. All these assumptions cause uncertainty in the snow fraction estimates which are discussed in detail in Section 2.5.3.

Angular anisotropy inherent both to reflectance and NDSI of the land surface and snow as well as atmospheric effects increase with increasing solar and satellite zenith angles. As a result, the accuracy of snow fraction retrievals when both angles are large may degrade.

3.2. Potential Improvements

Implemented snow fraction algorithms can be generally improved in a number of ways. Characterization of the reflectance angular anisotropy may be improved by introducing a more sophisticated physically-based BRDF model. This approach however would still require validation and additional tuning of the BRDF model using real satellite observations. Adding more endmembers characterizing different surface cover types (.e.g., vegetated and non-vegetated) may also be beneficial for the snow fraction algorithm performance. Changing from two to multiple endmember unmixing algorithm however may make the retrievals less robust and add noise due to the spectral similarity of different end-members. This approach has been implemented with GOES-R ABI data but did not demonstrate a robust and consistent performance.

The principal improvement of the product would consists in estimating the true snow cover fraction on the ground along with the “viewable” snow fraction estimated with the developed technique. The latter however requires an accurate model to predict the masking effect of the forest cover or a spatially distributed dataset directly characterizing this forest cover property.

4. REFERENCES

Barton, J. S., Hall, D. K., and Riggs, G. A. (2001). Remote sensing of fractional snow cover using moderate resolution imaging spectroradiometer (MODIS) data. Proceedings of the 57th Eastern Snow Conference, May 17–19, 2000, Syracuse, NY , pp. 171–183.

GSegDPS (2019) Joint Polar Satellite System (JPSS) Ground Segment Data Product Specification, https://www.jpss.noaa.gov/assets/pdfs/technical_documents/474-01543_JPSS-GSegDPS_A.pdf

JPSS (2015) Joint Polar Satellite System (JPSS) Calibration/Validation Plan for Fractional Snow Cover Product , Version 1.2 DRAFT, 29 p.

Metsämäki, S. J., Anttila, S. T., Markus, H. J., & Vepsäläinen, J. M. (2005). A feasible method for fractional snow cover mapping in boreal zone based on a reflectance model. Remote Sensing of Environment, 95, 77–95.

Nolin, A.W., Dozier, J. and Mertes, L., 1993. Mapping alpine snow using a spectral mixture modeling technique, Ann. Glacier., 17, pp. 121-124.

Painter T.H. et al. (2009) Retrieval of subpixel snow covered area, grain size, and albedo from MODIS. Remote Sensing of Environment 113: 868-879.

Riggs, George A., Dorothy K. Hall, and Miguel O. Roman. 2015. VIIRS Snow Cover Algorithm Theoretical Basis Document. https://modis-snow-ice.gsfc.nasa.gov/uploads/VIIRS_snow_cover_ATBD_2015.pdf.

Rittger, K., T. H. Painter, and J. Dozier (2013), Assessment of methods for mapping snow cover from MODIS, Adv. Water Resour., 51, 367–380.

Romanov P., D. Tarpley, G. Gutman and T.Carroll (2003) Mapping and monitoring of the snow cover fraction over North America. Journal of Geophysical Research, D108, 8619, doi:10.1029/2002JD003142, 2003

Salomonson, Appel (2004) Estimating Fractional Snow Cover From MODIS Using the Normalized Difference Snow Index (NDSI). Remote Sensing of the Environment 89:351-360.

Vikhamar, D., and Solberg, R. (2003). Snow-cover mapping in forests by constrained linear spectral unmixing of MODIS data. Remote Sensing of Environment, 88(3), 309−323. doi:10.1016/j.rse.2003.06.004

Xin, Q., Woodcock, C. E., Liu, J., Tan, B., Melloh, R. a, & Davis, R. E. (2012). View angle effects on MODIS snow mapping in forests. Remote Sensing of Environment, 118, 50–59.

END OF DOCUMENT